Electronic Supplementary Material (ESI) for Nanoscale. This journal is © The Royal Society of Chemistry 2020

Supporting Information

Multi-praseodymium-and-tungsten bridging octameric tellurotungstate and its 2D honeycomb composite film for detecting estrogen

Yan Zhang, Jun Jiang, Yifan Liu, Pan Li, Yong Liu, Lijuan Chen,* and Junwei Zhao*

Henan Key Laboratory of Polyoxometalate Chemistry, College of Chemistry and Chemical Engineering, Henan University, Kaifeng, Henan 475004, China.
* Corresponding authors: ljchen@henu.edu.cn, zhaojunwei@henu.edu.cn

Electronic Supplementary Information

Table S1. Crystallographic data and structure refinements for **1**.

Fig. S1 (a) Representation of the three-shell RE_{14}-substituted $[(RE_{14}(H_2O)W_4(OH)O_{14})(WO_4)_4(GeW_{10}O_{38})_6]^{43-}$ cluster. (b) The innermost shell of the $\{W_4O_{15}\}$ cluster.

Fig. S2 (a) The monocapped square antiprismatic geometry of the $Pr1^{3+}$ cation in **1**. (b) The monocapped square antiprismatic geometry of the $Pr2^{3+}$ cation in **1**.

Fig. S3 (a) The 3D packing of **1a** with a −A−B−A−B− array viewed along the *a* axis. (b) The simplified layer A displaying two spatial orientations of **1a** anions viewed along the *a* axis. (c) The simplified layer B displaying two spatial orientations of **1a** anions viewed along the *a* axis. (d) The simplified packing of **1a** with a −A−B−A−B− array viewed along the *a* axis. (e) The 3D packing with a −A−B−A−B− array of **1** viewed along the *b* axis. (f) The layer A exhibiting two spatial orientations of **1a** anions viewed along the *b* axis. (g) The layer B exhibiting two spatial orientations of **1a** anions viewed along the *b* axis. (h) The simplified packing mode of **1a** with a −A−B−A−B− array viewed along the *b* axis. (i) The packing of **1a** in the *ab* plane. (j) The simplified packing mode of **1a** in the *ab* plane. (k) Hydrogen-bonding interaction between $[H_2N(CH_3)_2]^+$ cations and **1a** anions. (l) Enlarged hydrogen-bonding interaction between $[H_2N(CH_3)_2]^+$ cations and **1a** anions.

Fig. S4 (a) The TEM image of the honeycomb **1@DODA** composite material at the scale bar of 1 μm. (b) The TEM image of the honeycomb **1@DODA** composite material at the scale bar of 500 nm.

Fig. S5 (a) DPV curves of the glassy carbon electrodes (GCEs) before and after modified by using the **1@DODA** honeycomb film composite material. (b) CV curves of GCEs before and after modified by using the **1@DODA** honeycomb film composite material. (c) EIS curves of GCEs before and after modified by using the **1@DODA** honeycomb film composite material.

Fig. S6 (a) CV curves of the Au/**1@DODA** electrodes prepared by controlling the electrodeposition time for 20, 40, 60, 80, 100, 120 and 140 s, respectively. (b) EIS responses of the Au/**1@DODA** electrodes prepared by controlling the electrodeposition time for 20, 40, 60, 80, 100, 120 and 140 s, respectively. (c) CV curves of the Au/**1@DODA**-80s electrodes obtained by incubating different concentration of aptamer of E2. (d) EIS responses

of the Au/**1@DODA**-80s electrodes obtained by incubating different concentration of aptamer of E2.

Fig. S7 XPS spectra of Au/**1@DODA** and Apt/Au/**1@DODA** composites for (a) W, (b) O, (c) C, (d) Au and (e) S elements.

Fig. S8 IR spectra of **1**, **1@DODA** and DODA·Br.

Fig. S9 The TG curve of **1.**

Materials and physical instruments

K_2TeO_3, $Na_2WO_4 \cdot 2H_2O$, $Pr(NO_3)_3 \cdot 6H_2O$, 2,6-pyridinedicarboxylic acid, $(CH_3)_2SnCl_2$, CH_3CN, hydrochloric acid, dimethylamine hydrochloride, K_2CO_3, DODA·Br, $K_3[Fe(CN)_6]$, $K_4[Fe(CN)_6] \cdot 3H_2O$, tris and KNO_3 were purchased from Sparke Chemical Co. Ltd. (Zhengzhou, Henan). $HAuCl_4 \cdot 4H_2O$, MB and E2 were purchased from Aladdin Biochemical Technology Co. Ltd. (Shanghai, China). The E2 aptamer and the segmental complementary DNA with rich G content (cDNA) were obtain from Shanghai Sangon Biological Engineering Technological Co. Ltd. (Shanghai, China) with the following sequences:

aptamer of E2: 5'-SH-$(CH_2)_6$-TTT TTT TTT T GCT TCC AGC TTA TTG AAT TAC ACG CAG AGG GTA GCG GCT CTG CGC ATT CAA TTG CTG CGC GCT GAA GCG CGG AAG C-3'

cDNA: 5'-GGA GGA GGA GGA GGA GGA GGA GGA GGA GGA GGA GGA GGA G G CTT CCG CGC TTC AGC GCG CAG CAA-3'

cDNA and E2 were dissolved in 10.0 mM tris-HCl buffer solution (pH = 8.0) including 200.0 mM NaCl, 25.0 mM KCl, 10.0 mM $MgCl_2$ and 5 % ethanol. The low concentration solutions are obtained by dilution of a high concentration solution.

The C, H and N elements were analyzed on a Perkin–Elmer 2400–II CHNS/O analyzer. Inductively coupled plasma atomic emission spectrometry (ICP–AES) was performed on a Perkin–Elmer Optima 2000 ICP–AES spectrometer. IR spectra were carried out on a Perkin–Elmer FT–IR spectrometer in the range of 400–4000 cm^{-1}. The TG analysis was recorded on a Mettler–Toledo TGA/SDTA 851^e instrument under a flowing N_2 atmosphere with a heating rate of 10 °C min^{-1} from 25 to 800 °C. Scanning electron microscopy (SEM) images were recorded on a Hitachi S-4800 field-emission scanning electron microscope equipped with energy-dispersive spectrometer (EDS). Transmission electron microscopy (TEM) images were obtained on a JEM–2100 electron microscope operated at 200 kV. X-ray photoelectron spectra (XPS) were recorded on Thermo Scientific K-Alpha+ X-ray photoelectron spectrometer. All electrochemical measurements were researched on a CHI660D electrochemical workstation (CH Instruments) with a conventional three-electrode system, which consists of a modified glassy carbon electrode (GCE), a KCl-saturated Ag/AgCl reference electrode, and a platinum counter electrode. When optimizing the experimental conditions, the electrochemical performance of the modified GCE was tested in 1.00 mM $K_3[Fe(CN)_6]$/$K_4[Fe(CN)_6]$ solution that contains 0.1 M KCl. The effect of adding different concentration of cDNA and the detection of E2 were evaluated by CV and DPV in 50.0 mM tris-HCl buffer solution (pH = 7.0) that contains 20 mM KCl. The corresponding EIS was recorded in 1.0 mM $K_3[Fe(CN)_6]$/$K_4[Fe(CN)_6]$ solution that contains 0.1 M KCl. When optimizing and detecting E2, the instrumental parameters: increment potential of each step is 0.004, amplitude is 0.05, pulse width is 0.005, sampling width is 0.0025, pulse period is 0.2.

X-ray crystallography

Single-crystal X-ray diffraction data of **1** were collected on a Bruker Apex II CCD diffractometer equipped with graphite-monochromated Mo Kα radiation (λ = 0.71073 Å) at 150 K. Routine Lorentz and polarization corrections were utilized and a multi-scan absorption correction was applied with the SADABS program.[1] Direct methods and refined on F^2 by full-matrix least-squares method were used to solve the structure and

locate the heavy atoms using the SHELXTL–97 program.[2,3] No hydrogen atoms associated with water molecules were located from the difference Fourier map. All non-hydrogen atoms were refined anisotropically except for some oxygen atoms and water molecules. According to the elemental analyses, ICP test and TG analyses, eight $[H_2N(CH_3)_2]^+$, four K^+, two Na^+ cations, ten protons and thirty-four lattice water molecules were directly added to the molecular formula of **1**. Crystallographic data and structural refinement parameters for **1** is demonstrated in Table S1. Crystallographic data and structure refinements for **1** reported in this paper have been deposited in the Cambridge Crystallographic Data Centre with CCDC 1973217. This data can be obtained free of charge from the Cambridge Crystallographic Data Centre via www.ccdc. cam.ac.uk/data_request/cif.

Table S1. Crystallographic data and structure refinements for **1**.

	1
Empirical formula	$C_{32}H_{318}K_8N_{16}Na_6O_{402}Pr_8Te_8W_{88}$
Formula weight	26138.64
Crystal system	Tetragonal
Space group	$I4_1/a$
a, Å	38.5523(9)
b, Å	38.5523(9)
c, Å	29.1596(8)
α, deg	90
β, deg	90
γ, deg	90
V, Å^{-3}	43339.3(19)
Z	4
D_c (g cm^{-1})	4.006
μ, mm^{-1}	24.849
$F(000)$	45824
T, K	150(2)
Limiting indices	$-36 \leq h \leq 45$
	$-46 \leq k \leq 33$
	$-34 \leq l \leq 32$
Reflections collected/unique	115107 / 19129
R_{int}	0.0458
Data/restrains/parameters	19129 / 2 / 1066
GOF on F^2	1.069
R_1, wR_2 ($I>2\sigma(I)$)[a]	0.0370, 0.0928
R_1, wR_2 (all data)	0.0416, 0.0957
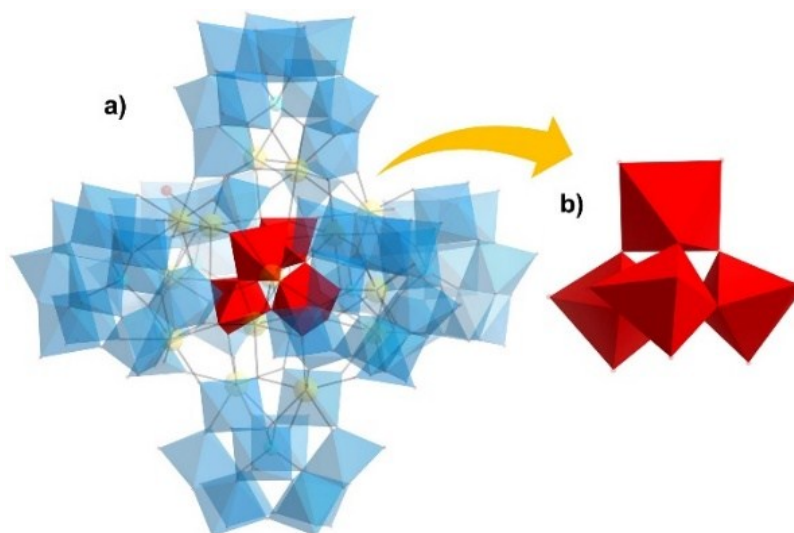
Fig. S1 (a) Representation of the three-shell RE$_{14}$-substituted [(RE$_{14}$(H$_2$O)W$_4$(OH)O$_{14}$)(WO$_4$)$_4$(GeW$_{10}$O$_{38}$)$_6$]$^{43-}$ cluster. (b) The innermost shell of the {W$_4$O$_{15}$} cluster.
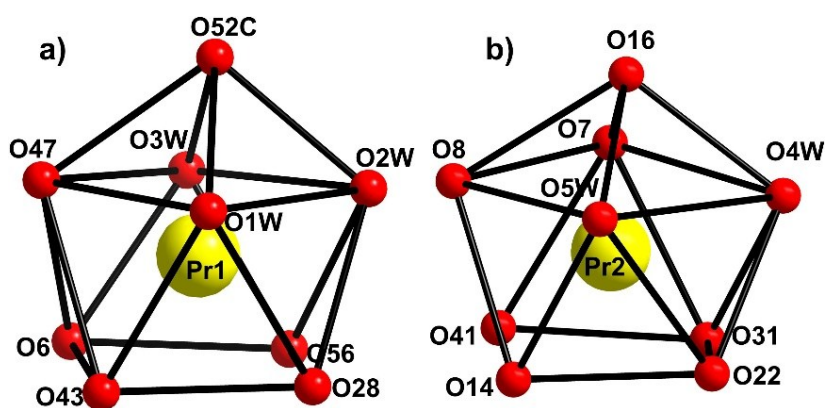

Fig. S2 (a) The monocapped square antiprismatic geometry of the Pr1^{3+} cation in **1**. (b) The monocapped square antiprismatic geometry of the Pr2^{3+} cation in **1**.

From the viewpoint of crystallography, there are two crystallographically independent Pr^{3+} cations (Pr1^{3+} and Pr2^{3+}) in the molecular unit of **1** (Fig. S2). Two crystallographically independent Pr^{3+} cations adopt the monocapped square antiprismatic geometry. In the coordination geometry of the Pr1^{3+} cation, O28 and O56 from the [B-α-TeW$_9$O$_{33}$]$^{8-}$ fragment and O6 and O43 from two {WO$_6$} bridges make up the bottom surface of the square antiprism while O1W, O2W, O3W and O47 in the {W5O$_6$} linker constitute the upper surface of the square antiprism. O52C from another [B-α-TeW$_9$O$_{33}$]$^{8-}$ fragment occupies the capping site of the square antiprism. In the coordination geometry of the Pr2^{3+} cation, it can be clearly seen that O14, O22, O31 and O41 atoms construct the bottom plane of the square antiprism while O7, O8, O4W and O5W define the upper plane of the square antiprism. O16 is located on the capping site of the distorted square antiprism.
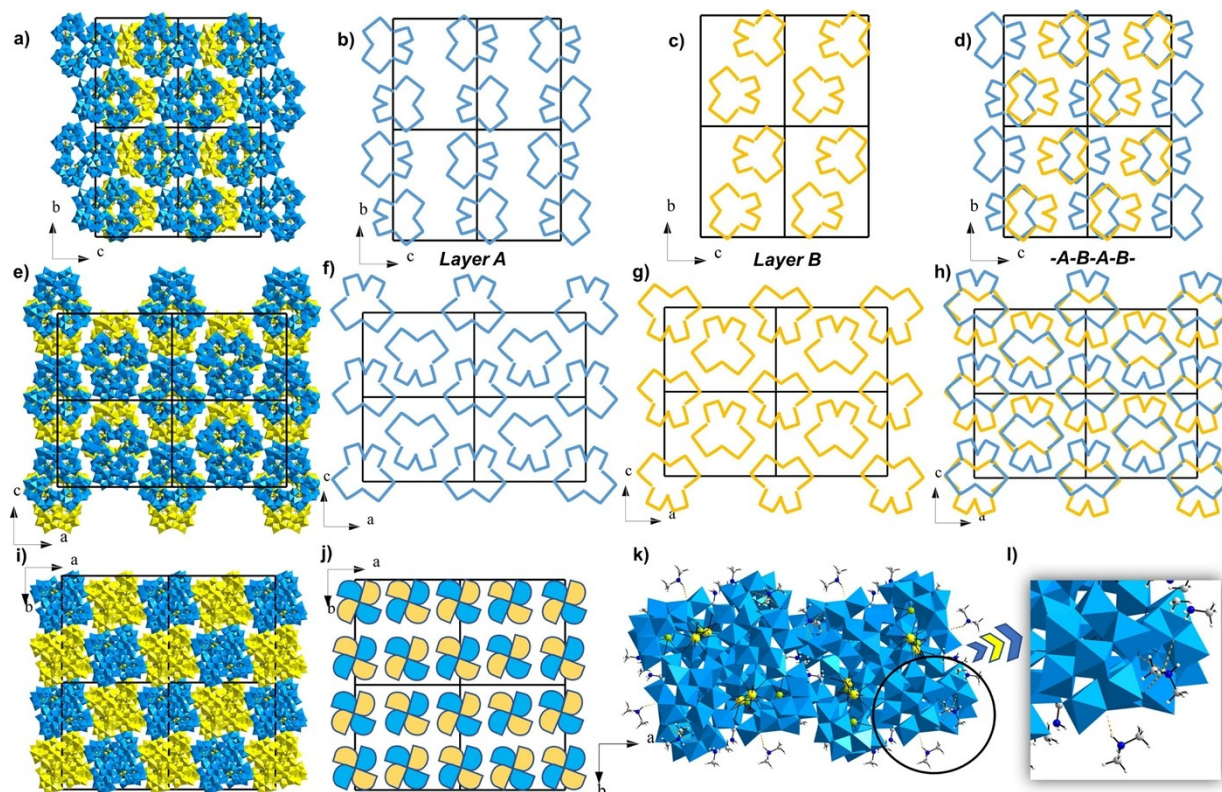
Fig. S3 (a) The 3D packing of **1a** with a −A−B−A−B− array viewed along the *a* axis. (b) The simplified layer A displaying two spatial orientations of **1a** anions viewed along the *a* axis. (c) The simplified layer B displaying two spatial orientations of **1a** anions viewed along the *a* axis. (d) The simplified packing of **1a** with a −A−B−A−B− array viewed along the *a* axis. (e) The 3D packing with a −A−B−A−B− array of **1** viewed along the *b* axis. (f) The layer A exhibiting two spatial orientations of **1a** anions viewed along the *b* axis. (g) The layer B exhibiting two spatial orientations of **1a** anions viewed along the *b* axis. (h) The simplified packing mode of **1a** with a −A−B−A−B− array viewed along the *b* axis. (i) The packing of **1a** in the *ab* plane. (j) The simplified packing mode of **1a** in the *ab* plane. (k) Hydrogen-bonding interaction between [$H_2N(CH_3)_2$]$^+$ cations and **1a** anions. (l) Enlarged hydrogen-bonding interaction between [$H_2N(CH_3)_2$]$^+$ cations and **1a** anions.
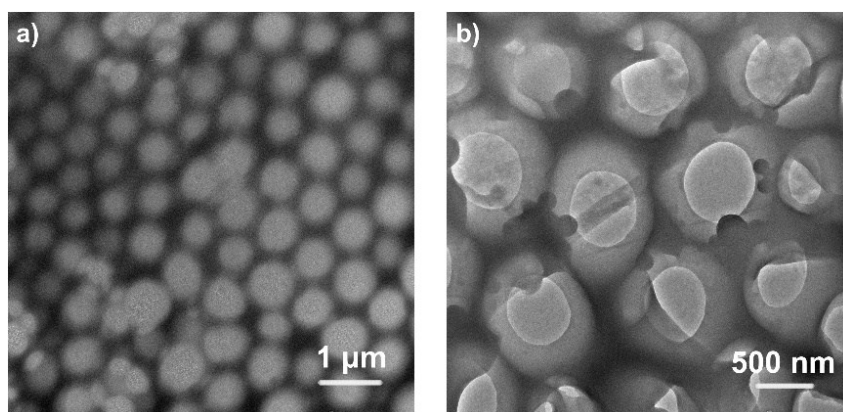

Fig. S4 (a) The TEM image of the honeycomb **1@DODA** composite material at the scale bar of 1 μm. (b) The TEM image of the honeycomb **1@DODA** composite material at the scale bar of 500 nm.
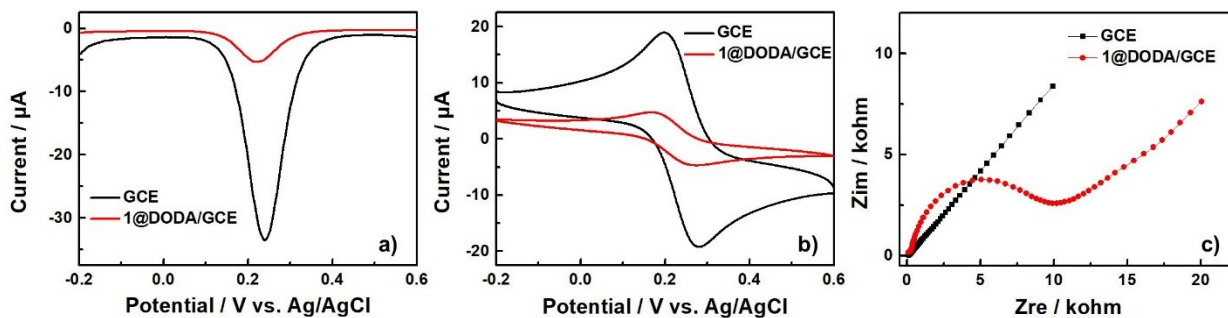
Fig. S5 (a) DPV curves of the glassy carbon electrodes (GCEs) before and after modified by using the **1@DODA** honeycomb film composite material. (b) CV curves of GCEs before and after modified by using the **1@DODA** honeycomb film composite material. (c) EIS curves of GCEs before and after modified by using the **1@DODA** honeycomb film composite material.
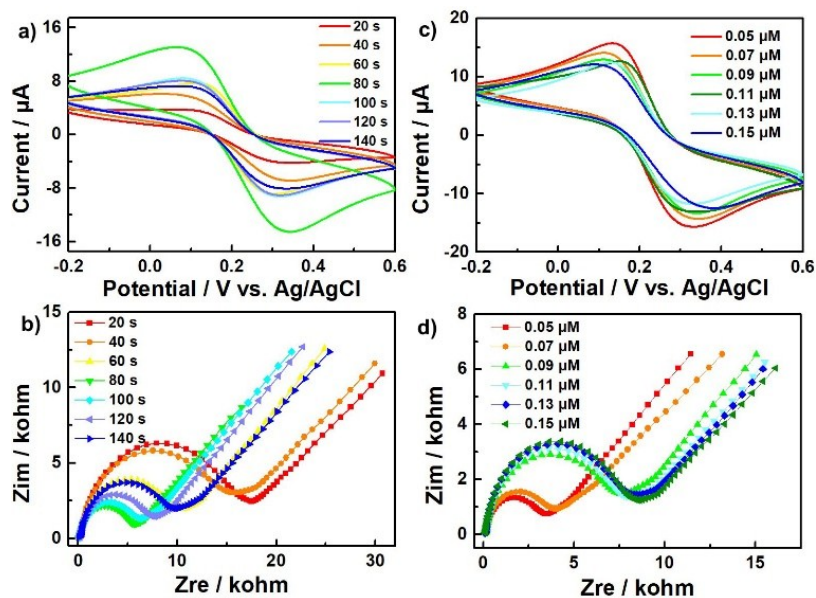

Fig. S6 (a) CV curves of the Au/**1@DODA** electrodes prepared by controlling the electrodeposition time for 20, 40, 60, 80, 100, 120 and 140 s, respectively. (b) EIS responses of the Au/**1@DODA** electrodes prepared by controlling the electrodeposition time for 20, 40, 60, 80, 100, 120 and 140 s, respectively. (c) CV curves of the Au/**1@DODA**-80s electrodes obtained by incubating different concentration of aptamer of E2. (d) EIS responses of the Au/**1@DODA**-80s electrodes obtained by incubating different concentration of aptamer of E2.
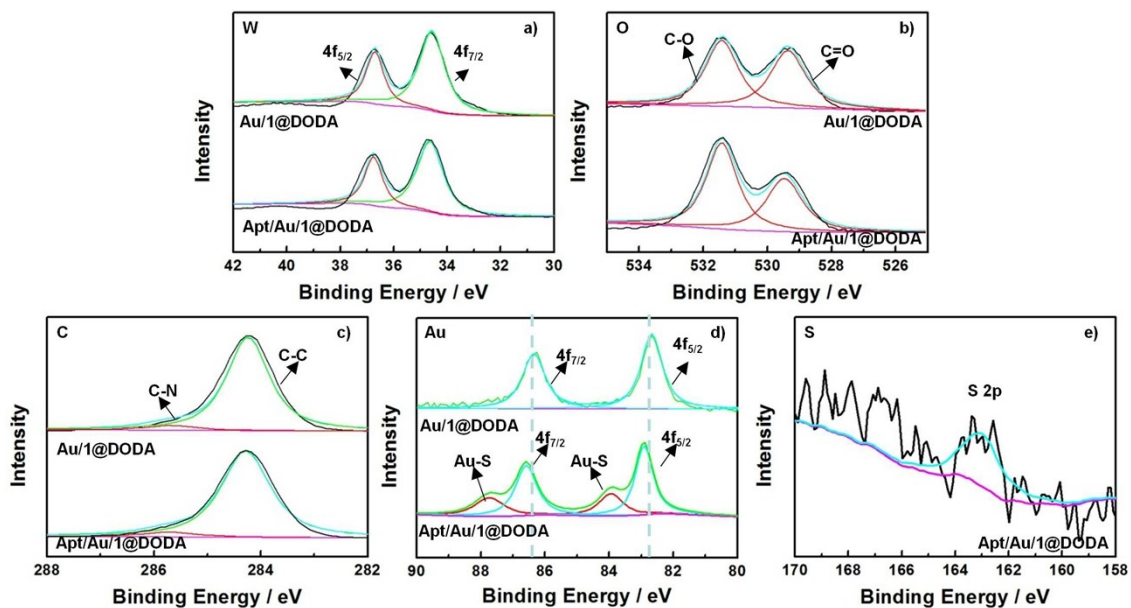
Fig. S7 XPS spectra of Au/**1@DODA** and Apt/Au/**1@DODA** composites for (a) W, (b) O, (c) C, (d) Au and (e) S elements.
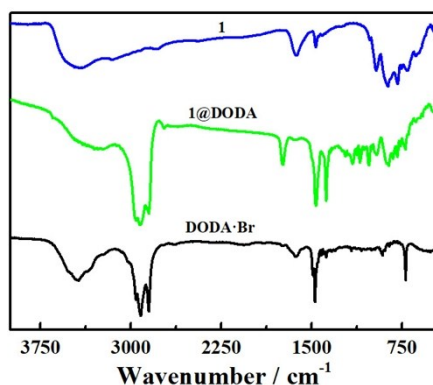

Fig. S8 IR spectra of **1**, **1@DODA** and DODA·Br.

In the IR spectrum of **1** (Fig. S8), it is obviously seen that the characteristic absorption peaks derived from the TT skeleton in the low wavelength range ($v < 1000$ cm^{-1}) appear at 965, 870 and 785 cm^{-1}, which respectively correspond to the v(W–O$_t$), v(W–O$_b$) and v(W–O$_c$) vibration bands. The absorption peak at 702 cm^{-1} is assigned to the v(Te–O) stretching vibration.[4,5] In the high wavenumber range ($v > 1000$ cm^{-1}), the resonances at 3142 and 2785 cm^{-1} are respectively attributed to the C–H and N–H stretching vibrations, indicating the existence of dimethylamine groups in **1**. In addition, the absorption band at 1620–1630 cm^{-1} is ascribed to the v(O–H) stretching vibration, proving the presence of water molecules in the structure.[5] In brief, the results of IR spectra are consistent with the single-crystal structural analysis of **1**. In the IR spectrum of **1@DODA** honeycomb film (Fig. S8). The characteristic absorption peaks of the TT skeleton appeared in the low wavelength range ($v < 1000$ cm^{-1}) and the C–H and N–H absorption peaks at 2960 and 2850 cm^{-1} resulting from the surfactant DODA$^+$ components, which indicates the successful composition of **1a** polyanions and DODA$^+$ components.
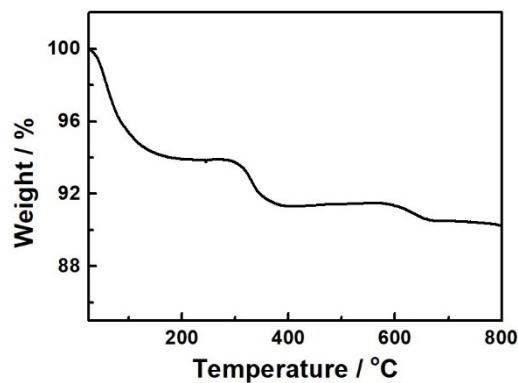
Fig. S9 The TG curve of **1.**

The thermal stability of **1** was measured under dry N_2 atmosphere in the range of 25–800 °C (Fig. S9). The TG curve of **1** exhibits a two-step weight loss process. In the range of 25–300 °C, the first weight loss of 6.26 % (clacd. 6.03 %) corresponds to the loss of seventy lattice water molecules and seven dimethylamine groups. With the temperature increasing to 800 °C, the second weight loss of 3.49 % (calcd. 3.82 %) is assigned to the removal of twenty coordination water molecules, nine dimethylamine groups and the dehydration of twenty-six protons.

References

1 G. M.Sheldrick, *SADABS: Program for Absorption Correction*; University of Göttingen: Göttingen, Germany, **1997**.

2 G. M.Sheldrick, *SHELXS 97, Program for Crystal Structure Solution,* University of Göttingen, Göttingen, Germany, **1997**.

3 G. M. Sheldrick, *SHELXL 97, Program for Crystal Structure Refinement*, University of Göttingen, Germany, **1997**.

4 Q. Han, Y. Wen, J.-C. Liu, W. Zhang, L.-J. Chen and J.-W. Zhao, *Inorg. Chem.,* 2017, **56**, 13228.

5 Y. Zhang, Y. M. Li, J. J. Pang, Y. F. Liu, P. Li, L. J. Chen and J. W. Zhao, *Inorg. Chem.,* 2019, **58**, 7078.